Fourier Transform Microwave Spectrum, Geometry, and Hyperfine Coupling Constants of Phosphenous Fluoride, OPF

Bethany Gatehouse,[†] Th. Brupbacher,[†] and Michael C. L. Gerry*

Department of Chemistry, The University of British Columbia, 2036 Main Mall, Vancouver, BC, V6T IZ1, Canada

Received: October 27, 1998

The microwave spectrum of phosphenous fluoride, OPF, has been measured using a pulsed-jet cavity Fourier transform microwave spectrometer. With the exception of a mass spectroscopic detection of the molecule, chemically prepared for use in a matrix IR study, this is the first observation of free gas-phase OPF. The samples were prepared from mixtures of PF_3 and O_2 in Ne carrier gas, using an electric discharge. Rotational transitions of two isotopomers ($^{16}O^{31}P^{19}F$ and $^{18}O^{31}P^{19}F$) have been measured in the 4−26 GHz frequency range. The determined rotational constants have been used to calculate r_0, r_z, and approximate r_e molecular geometries. In contrast to the nitrogen analogue, ONF, OPF has been found to show no irregularities in its geometry. Small hyperfine splittings due to the spin-1/2 ^{31}P and ^{19}F nuclei have been analyzed in terms of nuclear spin−rotation interactions. Because the determined coupling constants were of similar magnitudes and could not be unambiguously assigned, the related nuclear shielding parameters have been derived using both possible assignments. The spin−rotation coupling constants are compared with those calculated using ab initio techniques, and the ^{19}F nuclear shieldings are compared with those derived for the nitrogen analogue ONF.

Phosphenous fluoride, OPF, is a transient molecule that is the P analogue of nitrosyl fluoride, ONF. While the spectra of the nitrosyl halides ONX (X = F, Cl, Br) have been studied extensively by both microwave and infrared techniques,[1−13] studies on the phosphenous halides have rarely been reported. Indeed, the entire family of phosphenous halides[14−17] and the analogous arsenic-, antimony-, and sulfur-containing compounds, OAsCl,[18,19] OSbCl,[18,19] and SPX (X = F, Cl, Br),[20−22] have all been studied by only one group, using cryogenic matrix isolation infrared spectroscopy and ab initio calculations. A review of this work has been published.[23]

Characteristically, the nitrosyl halides are seen to have unusually long X−N bonds with a significant amount of ionic character. In addition, the electronegative halogen nuclei evidently withdraw electron density from the highest occupied molecular orbital, an antibonding orbital, of the N═O moiety, thus giving the nitrosyl halides shorter N═O bonds than that found in free NO. A similar situation applies for NSF (isoelectronic with OPF), which has an unusually long SF bond.[24,25] In contrast, the ab initio geometry and harmonic force field, as well as an estimated geometry, given for OPF in the earlier work[14,23] show little indication of such features; the PO and PF bond lengths are apparently similar to those of, for example, free PO and PF_3, respectively.

In the present work, pure rotational spectra of two isotopomers of OPF have been measured. The samples were prepared using electric discharges in PF_3/O_2 mixtures, and the transitions were observed using a pulsed jet cavity Fourier transform microwave (FTMW) spectrometer. This study represents the first observation of a spectrum of a free gas-phase phosphenous halide and the first direct experimental determination of its geometry. The rotational constants have been used to calculate r_0, r_z, and approximate r_e geometries. These parameters are compared with those obtained using ab initio techniques and with those of related species.

Some of the measured transitions were also observed to be split by nuclear hyperfine interactions. However, because both ^{19}F and ^{31}P have the same nuclear spin and the determined coupling constants were of similar magnitudes, the constants could not be assigned unambiguously to their respective nuclei. In an attempt to clarify this assignment ambiguity, the experimental spin−rotation coupling constants have been compared with those obtained using ab initio techniques. The absolute nuclear shielding parameters of both the ^{31}P and ^{19}F nuclei have been calculated from the determined spin−rotation coupling constants using both possible assignments. Those derived for the fluorine nucleus have been compared to those of the second-row analogue, ONF.

Experimental Details

The experiments were carried out in the 4−26 GHz frequency range using a Balle−Flygare-type[26] pulsed jet cavity spectrometer incorporating automated frequency scanning. This instrument has been described earlier.[27] In it, an inert carrier gas containing a small fraction of sample molecules, or their precursors, is injected into a microwave Fabry−Perot cavity cell as a pulsed supersonic expansion through a General Valve series 9 nozzle. Because the nozzle is located near the centre of one of the cavity mirrors and the jet travels parallel to the cavity axis, all observed lines are split into two Doppler components.

OPF was prepared by passing electric discharges through gas samples consisting of 0.5% PF_3 and 0.5% O_2 in roughly 5 bar Ne. The discharge apparatus, which is located at the front of

[†] Present address: Laboratorium für Physikalische Chemie, Eidgenössische Technische Hochschule, ETH Zentrum, CH-8092 Zürich, Switzerland.

10.1021/jp984202h CCC: $18.00
Published on Web 01/20/1999

the nozzle, has been described earlier.[28] The nozzle itself is mounted into one of the mirrors that form the microwave cavity cell. Because this mirror also acts as one of the vacuum chamber end flanges in the instrument used for these measurements, the discharge design has been slightly modified in order that the nozzle could be mounted outside the vacuum; the high voltage wires now have o-ring seals. The electrode design was also slightly modified from the previously used concentric discs. In order to avoid a strong capacitance between the electrodes, here small brass rectangles that overlapped only within the immediate area of the discharge were used at voltages of about 2−4 kV. To measure transitions of the ^{18}O isotopomer, a 50% ^{18}O-enriched O_2 sample, obtained from Cambridge Isotope Laboratories, was used.

Line frequencies were determined by fitting to the time domain signals,[29] and their uncertainties were estimated from the range of values resulting from each of several different measurements of each transition. In the particular case of the $3_{0,3}-2_{1,2}$ transition of ^{16}OPF, one of the hyperfine components has been given an uncertainty 4 times larger than that of the others. The position determined for this particular component showed a significantly larger variation between different measurements than did any of the other components (presumably because of its proximity to the much stronger transition), and its position was, therefore, considerably more uncertain.

Spectral Search and Analysis

The ab initio calculated geometry of ref 14 was first used to predict the rotational constants of the molecule and, from them, the frequencies of the rotational transitions. OPF is a planar asymmetric molecule with dipole moment components along both the *a* and *b* principal inertial axes; thus, its spectrum exhibits both *a*-type and *b*-type transitions. However, because of the large rotational constants and the low rotational temperature of the jet, there were few transitions available in the frequency range of the spectrometer. Initially, some *a*-type transitions were sought using the automated scanning capability; the scans were done using 256 signal averaging cycles and frequency increments of roughly 0.4 MHz. The initial scans were done in the region of the strong $J_{K_a,K_c} = 1_{0,1}-0_{0,0}$ transition. The regions 16 900−17 300 MHz and 16 800−16 900 MHz were scanned, and a transition was located at roughly 16 871.9 MHz; this transition showed hyperfine structure consistent with that of a molecule containing two spin-1/2 nuclei and was dependent upon the use of the discharge. It was assigned as the sought after $J_{K_a,K_c} = 1_{0,1}-0_{0,0}$ transition of OPF. A weaker transition was subsequently found at 5115.4 MHz after scanning the regions 5200−5400 MHz and 5100−5200 MHz; this transition was also seen to be discharge dependent and was assigned as being the Q-branch $J_{K_a,K_c} = 2_{1,1}-2_{1,2}$ transition. These two transitions were used to obtain initial values for the *B* and *C* rotational constants of the molecule.

To predict the *b*-type transitions, an estimate of the *A* rotational constant was required. This was obtained by first using the force constants and geometry of ref 14 to estimate the inertial defect. This and the *B* and *C* rotational constants determined above were then used to calculate *A.* From this calculated value, *b*-type transitions were predicted, and the strongest of these, $3_{0,3}-2_{1,2}$, was sought, again using the automated scanning. It was located within 60 MHz of the prediction. This transition was split into four hyperfine components, as was consistent with the proposed assignment.

All three rotational constants of the normal isotopomer could then be independently determined from the three observed transitions, and new transitions could be predicted with a reasonable degree of accuracy. Two more *a*-type Q-branch transitions of the normal isotopomer were thus easily found. A second *b*-type transition, $3_{2,2}-4_{1,3}$, predicted at 24 504.3 MHz, was also located, at roughly 24 503.98 MHz; however, it was very weak and had a correspondingly high uncertainty in its measured line position. This transition, therefore, was not included in the spectral fit; however, it did confirm the assignment of the first *b*-type transition.

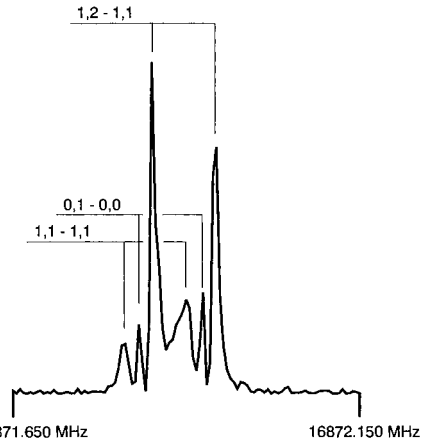

Figure 1. The $J_{K_a,K_c} = 1_{0,1}-0_{0,0}$ transition of ^{16}OPF, showing resolved hyperfine structure; the components are labelled according to the quantum numbers *I, F*. This spectrum was obtained using 128 signal averaging cycles and 4096 data points.

Rotational transitions for ^{18}OPF were located using a similar procedure. Preliminary rotational constants for this isotopomer were obtained by scaling those calculated from the ab initio geometry by the ratio between the measured and predicted constants of the main isotopomer; assignments of the measured transitions were confirmed by the similarity of the hyperfine structures to the analogous transitions of the ^{16}O isotopomer.

The rotational transitions of OPF showed some hyperfine structure due to nuclear spin−spin and nuclear spin−rotation interactions. Initially, in order to predict the expected hyperfine patterns, the nuclear spin−spin effects were completely neglected and the spin−rotation coupling constants were taken to be the scaled spin−rotation coupling constants of ONF. While these values were not expected to reproduce the observed hyperfine patterns (as had been seen before in many cases, the spin−rotation coupling constant of analogous molecules are often vastly different from one another[28,30,31]), they were thought to be useful, if only to give an idea of the relative strengths and the number of hyperfine components to expect in each transition. Using these predictions, the $1_{0,1}-0_{0,0}$ and $3_{0,3}-2_{1,2}$ transitions were expected to be split into one strong component plus two and three, respectively, similar intensity components, and all Q-branch transitions were expected to be split into two. While the predicted intensity pattern in the $1_{0,1}-0_{0,0}$ transition was in agreement with the observed spectrum, that of the $3_{0,3}-2_{1,2}$ transition was in distinct contrast with the measured spectrum, and for the Q-branch transitions only single lines were seen (the Q-branch transitions did, however, show a slight increase in line width with increasing *J*, thus indicating the presence of a small, nonresolvable hyperfine splitting). The $1_{0,1}-0_{0,0}$ transition of ^{16}OPF is shown in Figure 1, and the $3_{1,2}-3_{1,3}$ and $4_{1,3}-4_{1,4}$ transitions of ^{16}OPF are compared in Figure 2, where it can be seen that the linewidth shows a slight increase for the higher *J* transition.

The measured transitions were fit in several stages using Pickett's full-diagonalization fitting program SPFIT.[32] In the

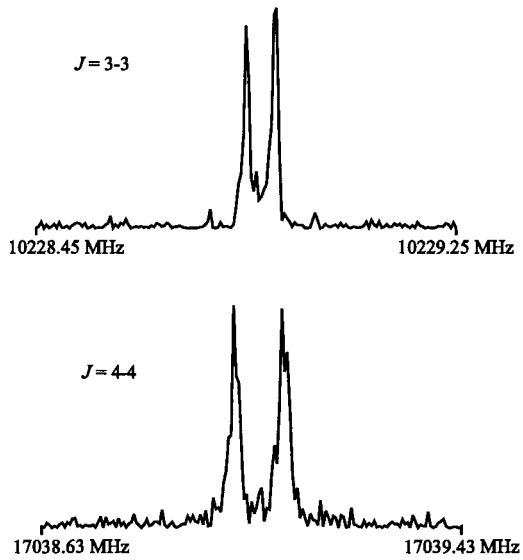

Figure 2. The $J_{K_a,K_c} = 3_{1,2}-3_{1,3}$ and $4_{1,3}-4_{1,4}$ transitions of ^{16}OPF, showing an increase in linewidth with increasing J: (upper trace) $3_{1,2}-3_{1,3}$ transition recorded using 512 signal averaging cycles; (lower trace) $4_{1,3}-4_{1,4}$ transition recorded using 1024 signal averaging cycles. Both traces consist of 4096 data points in the decay signal, corresponding to ~200 μs.

TABLE 1: Spin−Rotation Coupling Constant Dependence of the Observed Rotational Transitions of OPF

$2_{1,1}-2_{1,2}$	$3.0C_{bb}-3.0C_{cc}$
$3_{1,2}-3_{1,3}$	$6.0C_{bb}-6.0C_{cc}$
$4_{1,3}-4_{1,4}$	$10.0C_{bb}-10.0C_{cc}$
$1_{0,1}-0_{0,0}$	$1.0C_{bb}+1.0C_{cc}$
$3_{0,3}-2_{1,2}$	$4.6C_{bb}+2.4C_{cc}-1.0C_{aa}$

preliminary fits, the centrifugal distortion constants, with the exception of δ_J, were held fixed to the values obtained from the harmonic force field calculated using the data of ref 14; for the final spectroscopic fit, the centrifugal distortion constants were recalculated from the force field using the r_0 geometry determined here. The δ_J's of both ^{16}OPF and ^{18}OPF were fit as free parameters.

At first, weighted center frequencies of the rotational transitions were fit to the rotational and centrifugal distortion constants of the molecule. Then, hyperfine effects were considered. To this end, an r_0 molecular geometry was calculated using the rotational constants determined in the first fit and the nuclear spin−spin coupling constants were calculated using these geometrical parameters. These constants were included in all subsequent fits as fixed terms. The linear combinations of spin−rotation coupling constants to be used as fitting parameters were decided upon as follows.

The hyperfine splittings depend upon the rotational state-dependent spin−rotation constants, $C_{J,\tau}$, given by

$$C_{J,\tau} = \sum_g C_{gg}\langle J_g^{\,2}\rangle \qquad (1)$$

where g sums over the a, b, and c principal inertial axes and C_{gg} is the spin−rotation coupling constant along the g axis. Expressions for the $C_{J,\tau}$'s of all energy levels involved in the transitions measured here have been derived, and the dependence of each observed transition on the spin−rotation coupling constants is presented in Table 1. Here it is seen that the hyperfine splittings of the Q-branch transitions depend only upon the quantity $C_{bb}-C_{cc}$, the $1_{0,1}-0_{0,0}$ transition depends only on $C_{bb}+C_{cc}$, and the $3_{0,3}-2_{1,2}$ transition depends on all three spin−rotation coupling constants. Thus, the combinations of spin−rotation coupling constants best used as fitting parameters are $^1/_4(C_{bb}-C_{cc})$, $^1/_2(C_{bb}+C_{cc})$, and $C_{aa}-{}^1/_2(C_{bb}+C_{cc})$.

TABLE 2: Observed Transition Frequencies, ν, and Differences between Observed and Calculated Frequencies, Δ, of OPF

$J'_{K_a',K_c'} - J''_{K_a'',K_c''}$	I'	F'	I''	F''	^{16}OPF ν/MHz	^{16}OPF Δ/kHz	^{18}OPF ν/MHz	^{18}OPF Δ/kHz
$2_{1,1}-2_{1,2}$	1	3	1	3	5115.3930(20)	−0.3	4769.4710(20)	−0.1
	0	2	0	2				
	1	2	1	2				
	1	1	1	1				
$3_{1,2}-3_{1,3}$	1	4	1	4	10228.8764(20)	0.2	9537.2852(20)	0.1
	0	3	0	3				
	1	3	1	3				
	1	2	1	2				
$1_{0,1}-0_{0,0}$	1	1	1	1	16871.8598(10)	0.0	16013.2621(10)	0.0
	0	1	0	0	16871.8816(10)	0.0	16013.2829(10)	0.0
	1	2	1	1	16871.9000(10)	0.0	16013.3006(10)	0.0
$4_{1,3}-4_{1,4}$	1	5	1	5	17039.0464(20)	−0.1	15587.6318(20)	0.0
	0	4	0	4				
	1	4	1	4				
	1	3	1	3				
$3_{0,3}-2_{1,2}$	1	4	1	3	19397.2502(20)	−0.2	17665.7416(20)	0.0
	0	3	0	2	19397.2650(80)	3.1	17665.7520(20)	0.0
	1	3	1	2	19397.2751(20)	0.2	17665.7647(20)	0.0
	1	2	1	1	19397.2877(20)	−0.2	17665.7766(20)	0.0

In Table 1, it is seen that the splittings of the Q-branch transitions depend upon only $C_{bb}-C_{cc}$ and that the splittings should increase with increasing J; in this case, only a slight line broadening was observed, thus indicating that the quantity $C_{bb}-C_{cc}$ is very small. Thus, this fitting parameter was held fixed at a value of zero for both the fluorine and phosphorus nuclei. Starting values for the remaining spin−rotation fitting parameters were also needed. These were not taken to be the scaled spin−rotation coupling constants of ONF because these were not able to reproduce the observed intensity pattern in the hyperfine structure of the $3_{0,3}-2_{1,2}$ transition. Instead, starting values for the remaining spin−rotation fitting parameters were taken from ab initio calculations;[33] these values were seen to reflect the experiment in that the $^1/_4(C_{bb}-C_{cc})$ parameters were both seen to be very close to zero (roughly 1.8 kHz and −0.2 kHz for the F and P nuclei, respectively), and the intensity patterns predicted using the ab initio constants were in agreement with the observations. The individual hyperfine components of the split transitions were assigned according to this prediction, and a fit was made where the spin−rotation coupling constants were freed (within the constraint that, for both nuclei, $C_{bb}=C_{cc}$) and the spin−spin coupling constants were held fixed. Because the assignments of the similar intensity components were not unambiguous, other fits were also done where the assignments of the weaker components were systematically rotated through all possible combinations. The first assignment resulted in a fit with a root mean square (rms) standard deviation that was at least 1 order of magnitude smaller than that resulting from each of these other fits and was taken to be correct.

A complete listing of all measured transitions is given in Table 2, along with their assignments and the differences, Δ, between the measured and calculated line positions. The spectroscopic constants resulting from the final fit are given in Table 3, along with the fixed values used for the centrifugal distortion and nuclear spin−spin coupling constants. The rotational constants are precisely determined for both isotopomers. The centrifugal distortion constants δ_J are also well determined and agree well with the values estimated from the harmonic force field, which are also given in the table. The spin−rotation coupling constants are not particularly well

TABLE 3: Spectroscopic Constants of Phosphenous Fluoride[c]

	^{16}OPF	^{18}OPF
A/MHz	41886.65594(254)	40474.01757(237)
B/MHz	9288.59927(44)	8801.63625(44)
C/MHz	7583.31626(44)	7211.67738(44)
$\Delta_{(000)}$/uÅ^2	0.1696143(72)	0.1726115(79)
	(0.1666)[a]	(0.1696)[a]
Δ_J/kHz	8.52033[a]	7.69522[a]
Δ_{JK}/kHz	−86.7088[a]	−83.5791[a]
Δ_K/kHz	1083.77[a]	1026.03[a]
δ_J/kHz	2.4513(93)	2.2026(93)
	(2.42054)[a]	(2.17446)[a]
δ_K/kHz	23.2609[a]	20.5652[a]
S_{aa}(F−P)/kHz	−7.35	−7.35
S_{-}(F−P)/kHz	−4.30	−4.30

	scheme I	scheme II	scheme I	scheme II
C_{aa}(P)/kHz	103.(44)	110.(41)	99.(66)	103.(63)
C_{bb}(P)/kHz	16.5(39)[b]	19.1(31)[b]	16.3(61)[b]	17.8(53)[b]
C_{cc}(P)/kHz	16.5(39)[b]	19.1(31)[b]	16.3(61)[b]	17.8(53)[b]
C_{aa}(F)/kHz	110.(41)	103.(44)	103.(63)	99.(66)
C_{bb}(F)/kHz	19.1(31)[b]	16.5(39)[b]	17.8(53)[b]	16.3(61)[b]
C_{cc}(F)/kHz	19.1(31)[b]	16.5(39)[b]	17.8(53)[b]	16.3(61)[b]

[a] Harmonic force field values, obtained using the force constants of ref 14. [b] C_{bb} and C_{cc} were constrained to be equal in the fit. [c] Uncertainties (1σ) are given in parentheses.

determined, and their accuracy is also somewhat questionable because of the very small size of the data set used in their determination. Moreover, these constants could not be uniquely assigned to a particular nucleus because both nuclei have the same spin and coupling constants of a similar magnitude. In Table 3, both possible assignments have been included; these are labelled as "scheme I" and "scheme II".

Discussion

1. Molecular Geometry. In this work, the ground-state rotational constants of two isotopomers of OPF have been determined; these have been used to calculate an r_0 geometry for the molecule using the program RU111J.[34] Because OPF is a planar molecule, it has only two independent rotational constants; thus, the information from two isotopomers is sufficient to perform fits using many different combinations of data. This allows for an estimate of the uncertainty associated with the geometrical parameters; because the rotational constants have been determined to a high degree of precision, the uncertainties obtained from any one individual fit of these constants (or of the moments of inertia or planar moments of inertia derived from these constants) to the geometrical parameters are unrealistically small. By taking the average of several determinations and the standard deviation uncertainties thereof, r_0 geometrical parameters and reasonable estimates of the uncertainties can be obtained. Here, four different fits were done: a fit to all moments of inertia, a fit of only the I_b and I_c moments of inertia (chosen because their uncertainties were less than that associated with I_a), a fit of all planar moments of inertia, and a fit of only the P_a and P_b planar moments of inertia (chosen because of the planarity constraint). In all fits, the data were weighted according to the inverse squares of their uncertainties. Because the experimentally determined uncertainties in the rotational constants are almost identical for both isotopomers studied, no adjustments of the weights were necessary;[35] the experimental uncertainties aptly represent the quality of the data.

An r_z geometry has also been calculated for ^{16}O^{31}P^{19}F. For this purpose, a harmonic force field was required. This was taken to be that of ref 14 because it reproduced the inertial defects and δ_J values well (see Table 3) and because the new data obtained in this study were insufficient to make significant improvements. The ground-state average rotational constants (B_z) were obtained by subtracting the harmonic contributions to the α's from the measured rotational constants. The r_z geometry was evaluated by least-squares fitting to the B_z constants; the data were weighted according to the inverse squares of their uncertainties (taken to be the same as those for the ground-state constants). The isotopic variations in the bond lengths were accounted for using[36−38]

$$\delta r = -\frac{3}{2}a\delta\langle u^2\rangle - \delta K \qquad (2)$$

where the zero-point mean square amplitudes, $\langle u^2\rangle$, of the bonds and their perpendicular amplitudes, K, were obtained from the force field; the Morse parameters, a, were obtained from tabulated values.[39] The uncertainties given are those arising from the least squares fit.

An approximate equilibrium geometry was also calculated using[36−38]

$$r_e = r_z - \frac{3}{2}a\langle u^2\rangle + K \qquad (3)$$

and the r_z geometry. Here, the bond angle was assumed to be the same as that for the r_z geometry. The uncertainties in this geometry are hard to estimate, but are likely similar to those obtained for the averaged r_0 geometry.

The determined r_0, r_z, and r_e geometries are presented in Table 4 where they are compared with the ab initio geometrical parameters obtained in this study, using the program Gaussian 94[40] and with the ab initio parameters calculated in ref 14. Here, it is seen that the experimental geometries are in agreement with one another and that they compare well with the geometrical parameters calculated using theoretical means, with the best estimate being that of the CPF geometry of ref 14. The overall "estimate" of the geometry in ref 14 (p 7910), from the CPF

TABLE 4: Geometrical Parameters of OPF

type	fit to	r(P═O)/Å	r(P−F)/Å	∠(OPF)/deg
r_0	I_a, I_b, I_c	1.452 725(1)[a]	1.576 210(1)[a]	110.391 243(8)[a]
r_0	I_b, I_c	1.456 157(1)[a]	1.578 531(1)[a]	110.005 260(13)[a]
r_0	P_a, P_b, P_c	1.452 725(1)[a]	1.576 210(1)[a]	110.391 243(8)[a]
r_0	P_a, P_b	1.454 408(1)[a]	1.578 406(1)[a]	110.224 908(9)[a]
r_0	averaged	1.454 0(16)[a]	1.577 3(13)[a]	110.25(18)[a]
r_z	A_z, B_z, C_z	1.456 43(22)[b]	1.577 66(22)[b]	110.2515(26)[b]
r_e	approx geometry	1.453 4[c]	1.573 3[c]	110.25[c]
	ab Initio Results			
Gaussian 94				
	SCF(6-31G*)	1.4369	1.5727	109.301
	SCF(D95V*)	1.4479	1.5953	108.390
	SCF(D95V+(3df,2p))	1.4254	1.5495	109.410
previous work[14]				
	SCF	1.426	1.549	109.9
	CI(SD)	1.440	1.559	109.7
	CPF	1.456	1.576	110.0

[a] For the r_0 values from individual fits (top four entries), the uncertainties are 1σ standard deviations obtained from the specific fits. For the averaged r_0 geometry, the uncertainties are 1σ, standard deviations obtained via averaging the individual determinations. [b] r_z geometry for ^{16}O^{31}P^{19}F. The uncertainties are the 1σ values from the least- squares fit. [c] Though the uncertainties of the r_e parameters are unknown, they are probably similar to those of the averaged r_0 parameters.

TABLE 5: Comparison of the Geometrical Parameters of OPF with Those of Related Species

	ref		r(P/N═O)/Å	r(P/N−F/H)/Å	∠/deg
OPF		r_0	1.4540(16)	1.5773(13)	110.25(18)
OPH	53	r_0	1.480(5)	1.456(3)	103.5(25)
OPF_3	54	r_e	1.436(6)	1.524(3)	
PF_3	55	r_e		1.563(2)	
PO	56	r_e	1.431		
ONF	4	r_e	1.13146(44)	1.51666(46)	109.919(14)
ONH	57	r_0	1.212(1)	1.063(2)	108.6(2)
ONF_3	58	r_a	1.158(4)	1.431(3)	
NF_3	59	r_e		1.3648(20)	
NO	60	r_e	1.151		

	ref		r(O/N═S)/Å	r(S/Si−F)/Å	∠/deg
SiF_2	61	r_e		1.5901(1)	100.77(2)
SO_2	62	r_e	1.43076(13)		119.33(1)
NSF	24	r_s	1.448(2)	1.643(2)	116.91(8)
SF_4 eq	63	r_e		1.545(3)	
ax				1.646(3)	
SN	64	r_e	1.4938(2)		

geometries of OPF and NSF, the experimental geometry of NSF, and "the authors' general experience", also agree well with our results. In general, the differences between the experimental and calculated geometries are very small.

A comparison of the geometrical parameters of OPF, ONF, and related molecules is given in Table 5. It is seen that in ONF the N−F bond is very long in comparison to that of NF_3 and that the N═O bond is somewhat shorter than that of the free NO species. Similar trends are also found for ONCl,[5] but they are not reflected by OPF. It is seen in Table 5 that the P═O and P−F bond lengths determined for OPF are very similar to those of the PF_3 and PO species. Interestingly, the ONH and ONF_3 species show bond length trends that are similar to those of the OPH and OPF_3 species, indicating that it is ONF, and not OPF, that is somewhat unusual. The experimentally determined OPF geometrical parameters support the conclusion drawn by Ahlrichs et al.[14] that OPF does not share many similarities with the nitrosyl halides and that its structural parameters are better compared with those of the isoelectronic species SiF_2, SO_2, and NSF.

A structural comparison between OPF and the related molecules SiF_2, SO_2, and NSF is also presented in Table 5. The bond angle of OPF is seen to be intermediate between those of SiF_2 and SO_2, as might be expected from a consideration of the relative positions of the Si, P, and S nuclei in the periodic table. NSF, however, has a somewhat shorter N═S bond than does free NS and an S−F bond length of a similar magnitude to that of the axial S−F bond of SF_4, which is, in itself, an atypically long bond.[25] Apparently, NSF has a bonding situation that is intermediate between that of phosphenous fluoride and nitrosyl fluoride.

2. Nuclear Spin−Rotation Coupling Constants. The spin−rotation coupling constants determined for OPF are given in Table 3. Because the determined constants were of a very similar magnitude for both of these spin-1/2 nuclei, it was impossible to assign a particular set of values to a particular nucleus based on the experimental evidence; accordingly, in the table, both possible assignments are included.

The spin−rotation coupling constants of OPF had been calculated using the program Dalton[41] in the hope that perhaps the ab initio predicted coupling constants could be used to allow for a positive assignment of the observed hyperfine structure. It was also hoped that, once this hyperfine structure had been assigned and analyzed, the ab initio calculations could provide a basis used to assign the measured spin−rotation coupling constants to their respective nuclei. The calculations have been performed at the experimentally determined r_0 geometry using a singles and doubles multireference restricted active space multiconfiguration self-consistent field (RAS-MCSCF) wavefunction under various different basis sets. The inactive space consisted of all core and inner valence orbitals, and the active space consisted of the remaining strongly occupied orbitals plus their correlating orbitals. Only a single correlating orbital was included for each strongly occupied orbital held within the active space; a consideration of the MP2 natural orbital occupation numbers indicated that this choice of active space should sufficiently account for dynamical correlation effects.[42,43] This active space was further divided into two parts: the fully active RAS2 space (electron excitations both into and out of these orbitals are allowed) contained the strongly occupied orbitals plus two rather strongly occupied (multireference) correlating orbitals and the limited activity RAS3 space (only electron excitations into these orbitals are allowed) contained the remaining correlating orbitals. Details on the calculations can be found in ref 33.

In Table 6, the experimental and ab initio spin−rotation coupling constants are compared. Both assignments of the measured values are seen to be in relatively good agreement with the calculations, especially when the large uncertainties associated with these constants are taken into account; this comparison cannot be used to help clarify the assignment ambiguity. A comparison of the relative magnitudes of the spin−rotation coupling constants is also not really informative; whereas in the ab initio calculation, the C_{aa} constant for the phosphorus nucleus is larger and the $^1/_2(C_{bb} + C_{cc})$ parameter is smaller than the corresponding quantities for the fluorine nucleus, the measured values pair the larger C_{aa} with the larger $^1/_2(C_{bb} + C_{cc})$. In order to make a strong argument in favor of one or the other of the two possible spin−rotation coupling constant assignments, more experimental work is clearly needed. With the measurement of more transitions showing hyperfine structure (many of which lie in the 25−40 GHz frequency range; outside of the operating frequency range of the spectrometer used for this work), not only could the spin−rotation coupling constants be determined with a greater accuracy and precision but it might also be possible to separate the contributions from the *b* and *c* components. On the basis of the ab initio results, it is possible that the relative magnitudes of C_{bb} and C_{cc} could be used to distinguish between the two nuclei.

3. Absolute Nuclear Shielding Parameters. The spin−rotation constants of a nucleus A can be written as the sum of a nuclear and an electronic term[44−48]

$$C_{gg}^{A} = C_{gg}^{A}(\text{nuc}) + C_{gg}^{A}(\text{el}) \tag{4}$$

where the two terms are given by

$$C_{gg}^{A}(\text{nuc}) = \frac{-2e\mu_N g^A B_{gg}}{\hbar c} \sum_{n \neq A} Z_n \frac{r_{nA}^2 - (r_{nA})_{gg}^2}{r_{nA}^3} \tag{5}$$

$$C_{gg}^{A}(\text{el}) = \frac{2e\mu_N g^A B_{gg}}{\hbar cm} \sum_k \frac{\langle 0|\sum_i L_{i,gA}|k\rangle\langle k|\sum_i L_{i,gA}/r_{iA}^3|0\rangle + \text{cc}}{E_k - E_0} \tag{6}$$

Here μ_N is the nuclear magneton, g^A is the *g* factor of nucleus A, *e* and *m* are the proton charge and electron mass, *c* is the speed of light, r_{nA} is the distance between nucleus *n*, of atomic

TABLE 6: Comparison of the Experimental and ab Initio Fluorine and Phosphorus Spin−Rotation Constants (kHz) of OPF

	P			F		
	C_{aa}	C_{bb}	C_{cc}	C_{aa}	C_{bb}	C_{cc}
			ab Initio			
^{16}OPF						
6-31G*	94.0	12.9	13.5	84.6	17.9	11.3
aug-cc-pVDZ	95.5	12.8	13.3	83.6	17.9	10.9
aug-cc-pVTZ	100.6	13.8	14.5	84.9	18.1	12.1
^{18}OPF						
6-31G*	90.7	12.2	12.2	81.7	17.0	10.7
aug-cc-pVDZ	92.3	12.2	12.7	80.7	17.0	10.4
aug-cc-pVTZ	97.2	13.1	13.8	80.1	17.2	11.5
			Experiment			
^{16}OPF						
scheme I	103.(44)	16.5(39)[a]	16.5(39)[a]	110.(41)	19.1(31)[a]	19.1(31)[a]
scheme II	110.(41)	19.1(31)[a]	19.1(31)[a]	103.(44)	16.5(39)[a]	16.5(39)[a]
^{18}OPF						
scheme I	99.(66)	16.3(61)[a]	16.3(61)[a]	103.(63)	17.8(53)[a]	17.8(53)[a]
scheme II	103.(63)	17.8(53)[a]	17.8(53)[a]	99.(66)	16.3(61)[a]	16.3(61)[a]

[a] C_{bb} and C_{cc} were constrained to be equal in the fits.

TABLE 7: Derived[a] ^{19}F and ^{31}P Nuclear Shielding Parameters (ppm) of OPF

	^{16}OPF				^{18}OPF			
	scheme I		scheme II		scheme I		scheme II	
	P	F	P	F	P	F	P	F
σ_{aa}(d)	1021(5)[b]	518(5)[b]	1021(5)[b]	518(5)[b]	1021(5)[b]	518(5)[b]	1021(5)[b]	518(5)[b]
σ_{bb}(d)	1067(5)[b]	613(5)[b]	1067(5)[b]	613(5)[b]	1067(5)[b]	613(5)[b]	1067(5)[b]	613(5)[b]
σ_{cc}(d)	1111(5)[b]	640(5)[b]	1111(5)[b]	640(5)[b]	1111(5)[b]	640(5)[b]	1111(5)[b]	640(5)[b]
σ_{av}(d)	1066(3)[b]	590(3)[b]	1066(3)[b]	590(3)[b]	1066(3)[b]	590(3)[b]	1066(3)[b]	590(3)[b]
σ_{aa}(p)	−1049(426)	−492(171)	−1117(397)	−463(183)	−1044(662)	−477(272)	−1084(631)	−460(284)
σ_{bb}(p)	−827(170)	−505(58)	−940(135)	−456(73)	−857(281)	−499(105)	−926(244)	−469(121)
σ_{cc}(p)	−1040(209)	−618(71)	−1180(166)	−560(90)	−1075(343)	−610(128)	−1159(298)	−574(148)
σ_{av}(p)	−972(168)	−539(65)	−1079(150)	−493(72)	−992(266)	−529(106)	−1057(247)	−501(114)
σ_{aa}	−28(426)	27(171)	−96(397)	56(184)	−23(662)	41(272)	−63(631)	58(285)
σ_{bb}	241(170)	108(59)	127(136)	157(74)	210(281)	114(105)	141(244)	144(121)
σ_{cc}	70(209)	20(72)	−69(166)	80(90)	36(343)	29(128)	−49(298)	65(148)
σ_{av}	94(168)	52(65)	−13(150)	98(72)	74(266)	61(106)	10(247)	89(114)

[a] C_{bb} and C_{cc} were constrained to be equal in the fit. [b] Estimated uncertainty.

number Z_n, and nucleus A, $L_{i,gA}$ is the g component of the orbital angular momentum of electron i about nucleus A, r_{iA} is the distance between electron i and nucleus A, and $|0\rangle$ and $|k\rangle$ are the ground- and excited-state electronic wave functions, at energies E_0 and E_k, respectively. Thus, the nuclear term, C^A_{gg}(nuc), is seen to depend only on the geometry of the molecule, whereas in order to calculate the electronic term, C^A_{gg}(el), one requires knowledge of the ground- and excited-state wave functions and their energies.

The electronic contributions to the spin−rotation coupling constants are related to the paramagnetic parts of the nuclear shielding parameters by

$$\sigma^A_{gg}(p) = \frac{-e\hbar C^A_{gg}(el)}{4mc\mu_N g^A B_{gg}} \quad (7)$$

and the diamagnetic shieldings can be approximately expressed in terms of the nuclear contributions to the spin−rotation coupling constants as[44]

$$\sigma^A_{gg}(d) = \sigma^A_{free}(d) - \frac{e\hbar}{4mc\mu_N g^A B_{gg}} C^A_{gg}(nuc) + \frac{e^2}{2mc^2}\sum \frac{3(r_{nA})_{gg}^2 - r_{nA}^2}{r_{nA}^5}\left\langle\frac{\rho^2}{3}\right\rangle_n \quad (8)$$

where $\sigma^A_{free}(d)$ is the free atom diamagnetic susceptibility, and $\langle\rho^2/3\rangle_n$ is the average squared electronic distance from nucleus n; these are obtained from tabulated values in refs 49 and 50, respectively. The components of the total shielding are given by

$$\sigma^A_{gg} = \sigma^A_{gg}(d) + \sigma^A_{gg}(p) \quad (9)$$

The nuclear and electronic contributions to the spin−rotation coupling constants of OPF were derived using eqs 4−6, the averaged r_0 geometrical parameters given in Table 4, and the measured coupling constants given in Table 3; because the measured spin−rotation constants could not be unambiguously assigned to their respective nuclei, these calculations have been done using both possible assignments. The nuclear shielding parameters of OPF were then derived from these using eqs 7−9. The results are compiled in Table 7, where the labels "scheme I" and "scheme II" are consistent with those used in Table 3. In Table 7, it can be seen that the individual paramagnetic shielding terms are fairly well determined, with the largest uncertainties being roughly half the magnitude of the associated values, and the diamagnetic terms, being calculated values that depend on only ground-state parameters, are, relatively speaking, very accurately "determined", with deemed uncertainties being well below 1% of the associated values. Because the overall nuclear shielding terms (σ_{gg} and σ_{av}) are obtained by adding these two contributions (both large numbers of opposite sign), they are completely indeterminate with uncertainties of at least

TABLE 8: Comparison of the Fluorine Nuclear Shielding Parameters (ppm) of OPF and ONF

	^{16}OPF		^{18}OPF		ONF
	scheme I	scheme II	scheme I	scheme II	
σ_{aa}(d)	518(5)[a]	518(5)[a]	518(5)[a]	518(5)[a]	492(5)[a]
σ_{bb}(d)	613(5)[a]	613(5)[a]	613(5)[a]	613(5)[a]	572(5)[a]
σ_{cc}(d)	640(5)[a]	640(5)[a]	640(5)[a]	640(5)[a]	582(5)[a]
σ_{av}(d)	590(3)[a]	590(3)[a]	590(3)[a]	590(3)[a]	549(3)[a]
σ_{aa}(p)	−492(171)	−463(183)	−477(272)	−460(284)	−639(5)
σ_{bb}(p)	−505(58)	−456(73)	−499(105)	−469(121)	−1145(7)
σ_{cc}(p)	−618(71)	−560(90)	−610(128)	−574(148)	−840(8)
σ_{av}(p)	−539(65)	−493(72)	−529(106)	−501(114)	−875(4)
σ_{aa}	27(171)	56(184)	41(272)	58(285)	−146(7)
σ_{bb}	108(59)	157(74)	114(105)	144(121)	−574(9)
σ_{cc}	20(72)	80(90)	29(128)	65(148)	−258(10)
σ_{av}	52(65)	98(72)	61(106)	89(114)	−326(5)

[a] Estimated uncertainty.

TABLE 9: Nonzero Calculated Fluorine Paramagnetic Shielding Proportionalities, σ_p(ppm)$\Delta E(E_h)$, for OPF[a] and ONF[b]

	OPF		ONF	
σ_{aa}(p)	$13A' \rightarrow 4A''$	−65	$10A' \rightarrow 3A''$	−62
	$12A' \rightarrow 4A''$	−3	$9A' \rightarrow 3A''$	−11
	$11A' \rightarrow 4A''$	4	$8A' \rightarrow 3A''$	14
	$10A' \rightarrow 4A''$	8	$7A' \rightarrow 3A''$	1
	$3A'' \rightarrow 14A'$	−20	$2A'' \rightarrow 11A'$	−28
	$2A'' \rightarrow 14A'$	−179	$1A'' \rightarrow 11A'$	−203
	$3A'' \rightarrow 15A'$	15	$2A'' \rightarrow 12A'$	−17
	$2A'' \rightarrow 15A'$	−20	$1A'' \rightarrow 12A'$	11
σ_{bb}(p)	$13A' \rightarrow 4A''$	0	$10A' \rightarrow 3A''$	−5
	$12A' \rightarrow 4A''$	−59	$9A' \rightarrow 3A''$	−60
	$11A' \rightarrow 4A''$	−20	$8A' \rightarrow 3A''$	23
	$10A' \rightarrow 4A''$	21	$7A' \rightarrow 3A''$	−17
	$3A'' \rightarrow 14A'$	36	$2A'' \rightarrow 11A'$	−53
	$2A'' \rightarrow 14A'$	−173	$1A'' \rightarrow 11A'$	−194
	$3A'' \rightarrow 15A'$	−73	$2A'' \rightarrow 12A'$	−31
	$2A'' \rightarrow 15A'$	13	$1A'' \rightarrow 12A'$	24
σ_{cc}(p)	$13A' \rightarrow 14A'$	26	$10A' \rightarrow 11A'$	24
	$12A' \rightarrow 14A'$	47	$9A' \rightarrow 11A'$	−118
	$11A' \rightarrow 14A'$	0	$8A' \rightarrow 11A'$	−311
	$10A' \rightarrow 14A'$	−369	$7A' \rightarrow 11A'$	−19
	$13A' \rightarrow 15A'$	15	$10A' \rightarrow 12A'$	8
	$12A' \rightarrow 15A'$	−34	$9A' \rightarrow 12A'$	4
	$11A' \rightarrow 15A'$	−55	$8A' \rightarrow 12A'$	2
	$10A' \rightarrow 15A'$	−2	$7A' \rightarrow 12A'$	−33

[a] OPF: HOMO $13A'$, LUMO $4A''$. [b] ONF: HOMO $10A'$, LUMO $3A''$.

approximately half the magnitude of the associated value and, at most, about 15 times the magnitude of the determined value.

Because the initial predicted values for the spin−rotation coupling constants of OPF, which were obtained by scaling those of ONF by the appropriate factors, were seen to produce a predicted intensity pattern that did not match that of the observed spectrum, it must be assumed that the spin−rotation coupling constants, and thus the corresponding nuclear shielding parameters, of these two fluorine nuclei are somewhat different. Therefore, to see where the differences arise, it is of interest to compare the absolute nuclear shielding terms derived for the fluorine nuclei of these two related molecules. The fluorine nuclear shielding parameters of ONF have been calculated using the spin−rotation coupling constants of ref 1 and the geometry of ref 2. These are compared to the derived fluorine nuclear shielding parameters of OPF in Table 8. Despite the differences in geometry, the diamagnetic shielding components are seen to be quite similar for both species; the majority of the difference in the nuclear shielding terms apparently comes from the differences in the paramagnetic shieldings. Such a result has been seen previously[28] when comparing the nuclear shielding parameters derived for the second- and third-row analogues SF_2 and OF_2.

The paramagnetic shielding terms usually have large negative values that counteract the large positive diamagnetic terms, resulting in moderate overall absolute shieldings.[51] In the case of SF_2, it was seen that the *a* and *b* principal inertial axis components of the paramagnetic shielding terms were quite small and, for that along the *a* axis, even positive.[28] For OPF, although the paramagnetic shielding terms are quite usual in that they have large negative values along each of the principal inertial axes, these values are each smaller than those of the corresponding term for ONF. In particular, the *b* axis fluorine paramagnetic shielding component of OPF is only about half the magnitude of that for ONF. This difference in paramagnetic shielding terms gives rise to a more positive fluorine shielding in OPF.

Although the paramagnetic shielding parameters of OPF and ONF can each be calculated using ab initio techniques,[33,52] such a comparison does not give any insight into the possible origin of the observed nuclear shielding differences. In the SF_2/OF_2 case, the difference in the nuclear shielding terms has been qualitatively explained in terms of the paramagnetic part of the shieldings using a simple equation[30] that allows one to estimate approximate values for the paramagnetic shielding terms. The equation to calculate the principal inertial *a* axis component of the paramagnetic shielding is given by[28]

$$\sigma_{aa}^{A}(p) = -8\beta^2\langle r^{-3}\rangle_{pA}\sum_j\sum_k \frac{(b_j^A c_k^A - c_j^A b_k^A)\sum_x (b_j^X c_k^X - c_j^X b_k^X)}{\Delta E_{j\rightarrow k}} \quad (10)$$

Corresponding expressions for the other components are obtained by cyclic permutations of the *a*, *b*, and *c* axes. In eq 10, $(r^{-3})_{pA}$ is the mean distance between the valence shell p-orbital electron and nucleus A; b_j, c_j and b_k, c_k are the LCAO coefficients of the valence shell p_b and p_c orbitals on a given atom for the molecular orbitals $|j\rangle$ and $|k\rangle$, respectively; X sums over all atoms in the molecule. Accordingly, if the atomic orbital contributions to the molecular orbitals and the energy differences between these molecular orbitals can be obtained, values for $\sigma_{gg}^{A}(p)$ can be estimated. Furthermore, this equation shows that the paramagnetic shielding terms are approximately proportional to a molecular orbital coefficient contribution and approximately inversely proportional to an electron excitation energy contribution. For the SF_2/OF_2 comparison, the main difference in the paramagnetic shielding terms was seen to arise because of a large difference in the electronic energy level structures. In both the SF_2 and OF_2 cases, the paramagnetic shielding terms along each principal inertial axis had only a single positive contribution. For the *a* and *b* components, the energies of these electron excitations for SF_2 were each less than half the magnitude of those for the corresponding OF_2 excitations, thus yielding very large, positive *a* and *b* contributions in the SF_2 case and much smaller positive *a* and *b* contributions in the OF_2 case. Although the energy gap corresponding to the positive contribution along the *c* axis for SF_2 was also smaller than that for OF_2, these energy differences were of a more similar magnitude than those giving rise to the positive *a* and *b* axis contributions. As a result, the differences between the *c* axis paramagnetic shielding components of these two related species were not as large as those between the *a* and *b* components.

Because the electronic structures of ONF and OPF are apparently rather different, it was a question of whether in this case the differences in the paramagnetic shielding terms were mainly due to large differences in the electronic energy level structures, or merely to large differences in the way in which the molecular orbitals are formed from the atomic orbitals. To this end, simple approximate atomic orbital contributions to the molecular orbitals have been obtained for OPF and ONF using the program Gaussian 94[40](MP2/STO-3G), and factors proportional to the individual paramagnetic shielding contributions ($\sigma_{gg}^{A}(p)\Delta E_{j\rightarrow k}$) were calculated using eq 10. These factors are given as "paramagnetic shielding proportionalities" in Table 9; here, all contributions from completely filled electron shells were found to be negligible and have not been included. In this table, it can be seen that the paramagnetic shielding proportionalities for analogous electronic excitations are quite similar for both molecules, thus suggesting that the paramagnetic shielding difference between OPF and ONF is likely largely due to differences in the energy level structures of the two molecules.

Acknowledgment. We thank Drs. R. Pomeroy and D. Sharma for supplying samples of PF_3. Support of this research from the Natural Sciences and Engineering Research Council (NSERC) of Canada is gratefully acknowledged. We acknowledge also the Petroleum Research Fund, administered by the American Chemical Society, for support of Th.B. during the course of this work.

References and Notes

(1) Styger, C.; Gatehouse, B.; Heineking, N.; Jäger, W.; Gerry, M. C. L. *J. Chem. Soc., Faraday Trans.* **1993**, *89*, 1899−1902.
(2) Buckton, K. S.; Legon, A. C.; Millen, D. J. *J. Chem. Soc., Faraday Trans.* **1969**, *65*, 1975−1984.
(3) Rohwer, F.; Guarnieri, A. *Z. Naturforsch., A* **1980**, *35*, 336−341.
(4) Cazzoli, G.; Degli Esposti, C. *Nuovo Cimento D* **1984**, *3*, 627−644.
(5) Gatehouse, B.; Müller, H. S. P.; Heineking, N.; Gerry, M. C. L. *J. Chem. Soc., Faraday Trans.* **1995**, *91*, 3347−3355.
(6) Cazzoli, G.; Cervellati, R.; Mirri, A. M. *J. Mol. Spectrosc.* **1975**, *56*, 422−431.
(7) Cazzoli, G.; C. Degli Esposti, P. P.; Simeone, G. *J. Mol. Spectrosc.* **1983**, *97*, 165−185.
(8) Millen, D. J.; Pannell, J. *J. Chem. Soc.* **1961**, 1322−1328.
(9) Roehrig, M. A.; Kukolich, S. *Mol. Phys.* **1992**, *76*, 221−227.
(10) Jones, L. H.; Ryan, R. R.; Asprey, L. B. *J. Chem. Phys.* **1967**, *49*, 581−585.
(11) McDonald, T. J. G. J. K.; Kalasinsky, V. F.; Geyer, T. J.; Durig, J. R. *J. Mol. Spectrosc.* **1988**, *132*, 104−122.
(12) Cheikh, M.; Alamichel, C. *Spectrochim. Acta, Part A* **1989**, *45A*, 153−157.
(13) Alamichel, C.; Verges, J. *Spectrochim. Acta, Part A* **1991**, *47A*, 915−918.
(14) Ahlrichs, R.; Becherer, R.; Binnewies, M.; Borrmann, H.; Lakenbrink, M.; Schunck, S.; Schnöckel, H. *J. Am. Chem. Soc.* **1986**, *108*, 7905−7911.
(15) Binnewies, M.; Lakenbrink, M.; Schnöckel, H. *High Temp. Sci.* **1986**, *22*, 83−94.
(16) Binnewies, M.; Lakenbrink, M.; Schnöckel, H. *Z. Anorg. Al1g. Chem.* **1983**, *497*, 7−12.
(17) Schnöckel, H.; Schunck, S. *Z. Anorg. Allg. Chem.* **1987**, *548*, 161−164.
(18) Binnewies, V. M. *Z. Anorg. Allg. Chem.* **1983**, *505*, 32−38.
(19) Schnöckel, H.; Lakenbrink, M.; Zhengyan, L. *J. Mol. Struct.* **1983**, *102*, 243−249.
(20) Schnöckel, H.; Schunck, S. *Z. Anorg. Allg. Chem.* **1987**, *552*, 163−170.
(21) Binnewies, V. M. *Z. Anorg. Allg. Chem.* **1983**, *507*, 66−69.
(22) Schnöckel, H.; Schunck, S. *Z. Anorg. Allg. Chem.* **1987**, *552*, 155−162.
(23) Binnewies, M.; Schnöckel, H. *Chem. Rev.* **1990**, *90*, 321−330.
(24) Cook, R. L.; Kirchhoff, W. H. *J. Chem. Phys.* **1967**, *47*, 4521−4527.
(25) Kuczkowski, R. L. *J. Am. Chem. Soc.* **1964**, *86*, 3617−3621.
(26) Balle, T. J.; Flygare, W. H. *Rev. Sci. Instrum.* **1981**, *52*, 33−45.
(27) Brupbacher, T.; Bohn, R. K.; Jiger, W.; Gerry, M. C. L.; Pasinszki, T.; Westwood, N. P. C. *J. Mol. Spectrosc.* **1997**, *181*, 316−322.
(28) Gatehouse, B.; Müller, H. S. P.; Gerry, M. C. *L. J. Chem. Phys.* **1997**, *106*, 6916−6922.
(29) Haekel, J.; Mäder, H. *Z. Naturforsch., A* **1988**, 43, 203−206.
(30) Cornwell, C. D. *J. Chem. Phys.* **1966**, *44*, 874−880.
(31) Muller, H. S. P.; Gerry, M. C. L. *J. Chem. Phys.* **1995**, *103*, 577−583.
(32) Pickett, H. M. *J. Mol. Spectrosc.* **1991**, *148*, 371−377.
(33) Gatehouse, B. To be published.
(34) Rudolph, H. D. *J. Mol. Spectrosc.* **1981**, *89*, 460−464.
(35) Rudolph, H. D. Accurate Molecular Structure from Microwave Rotational Spectroscopy. In *Advances in Molecular Structure Research*; Hargittai, I., Hargittai, M., Eds.; JAI Press: Greenwich, CT, 1996; pp 63−114.
(36) Kuchitsu, K. *J. Chem. Phys.* **1968**, *49*, 4456−4462.
(37) Kuchitsu, K.; Fukuyama, T.; Morino, Y. *J. Mol. Struct.* **1968**, *1*, 463−479.
(38) Kuchitsu, K.; Fukuyama, T.; Morino, Y. *J. Mol. Struct.* **1969**, *4*, 41−50.
(39) Kuchitsu, K.; Morino, Y. *Bull. Chem. Soc. Jpn.* **1965**, *38*, 805−813.
(40) Frisch, M. J.; Trucks, G. W.; Schlegel, H. B.; Gill, P. M. W.; Johnson, B. G.; Robb, M. A.; Cheeseman, J. R.; Keith, T.; Petersson, G. A.; Montgomery, J. A.; Raghavachari, K.; Al-Laham, M. A.; Zakrzewski, V. G.; Ortiz, J. V.; Foresman, J. B.; Peng, C. Y.; Ayala, P. Y.; Chen, W.; Wong, M. W.; Andres, J. L.; Replogle, E. S.; Gomperts, R.; Martin, R. L.; Fox, D. J.; Binkley, J. S.; Defrees, D. J.; Baker, J.; Stewart, J. P.; Head-Gordon, M.; Gonzalez, C.; Pople, J. A. *Gaussian 94*, revision b.3; Gaussian, Inc.: Pittsburgh, PA, 1995.
(41) Helgaker, T.; Jensen, H. J.; Jørgensen, P.; Olsen, J.; Ruud, K.; Aagren, H.; Andersen, T.; Bak, K. L.; Bakken, V.; Christiansen, O.; Dahle, P.; Dalskov, E. K.; Enevoldsen, T.; Fernandez, B.; Heiberg, H.; Hettema, H.; Jonsson, D.; Kirpekar, S.; Kobayashi, R.; Koch, H.; Mikkelsen, K. V.; Norman, P.; Packer, M. J.; Saue, T.; Taylor, P. R.; Vahtras, O. *Dalton release 1.0*, an electronic structure program; 1997.
(42) Aa. Jensen, H. J.; Jørgensen, P.; Agren, H.; Olsen, J. *J. Chem. Phys.* **1988**, *88*, 3834−3839.
(43) Aa. Jensen, H. J.; Jørgensen, P.; Agren, H.; Olsen, J. *J. Chem. Phys.* **1988**, *89*, 5354.
(44) Gierke, T. D.; Flygare, W. H. *J. Am. Chem. Soc.* **1972**, *94*, 7277−7283.
(45) Flygare, W. H.; Goodisman, J. *J. Chem. Phys.* **1968**, *49*, 3122−3125.
(46) Lo, M. K.; Weiss, V. W.; Flygare, W. H. *J. Chem. Phys.* **1966**, *45*, 2439−2449.
(47) Flygare, W. H. *J. Chem. Phys.* **1964**, *41*, 793−800.
(48) Ramsey, N. F. *Phys. Rev.* **1950**, *78*, 699−703.
(49) Malli, G.; Fraga, S. *Theor. Chim. Acta* **1966**, *5*, 275−283.
(50) Gierke, T. D.; Tigelaar, H. L.; Flygare, W. H. *J. Am. Chem. Soc.* **1972**, *94*, 330−338.
(51) Mason, J. *J. Chem. Soc. Dalton* **1975**, 1426−1431 and references therein.
(52) Gatehouse, B. *Chem. Phys. Lett.* **1998**, *288*, 698−704.
(53) Larzillière, M.; Damany, N.; My, L. T. *Chem. Phys.* **1980**, *46*, 401.
(54) Moritani, T.; Kuchitsu, K.; Morino, Y. *Inorg. Chem.* **1971**, *10*, 344−350.
(55) Hirota, E.; Morino, Y. *J. Mol. Spectrosc.* **1970**, *33*, 460−473.
(56) Coquart, B.; Prudhomme, J.-C. *C. R. Acad. Sci., Ser. B* **1972**, *275*, 383−385.
(57) Dalby, F. W. *Can. J. Phys.* **1958**, *36*, 1336−1371.
(58) Plato, V.; Hartford, W. D.; Hedberg, K. *J. Chem. Phys.* **1970**, *53*, 3488−3494.
(59) Otake, M.; Matsumura, C.; Morino, Y. *J. Mol. Spectrosc.* **1968**, *28*, 316−324.
(60) Gallagher, J.; Johnson, C. M. *Phys. Rev.* **1956**, *103*, 1727−1737.
(61) Shoji, H.; Tanaka, T.; Hirota, E. *J. Mol. Spectrosc.* **1973**, *47*, 268−274.
(62) Saito, S. *J. Mol. Spectrosc.* **1969**, *30*, 1−16.
(63) Tolles, W. M.; Gwinn, W. D. *J. Chem. Phys.* **1962**, *36*, 1119−1121.
(64) Amano, T.; Saito, S.; Hirota, E.; Morino, Y. *J. Mol. Spectrosc.* **1969**, *32*, 97−107.